NJC

Accepted Manuscript

This is an *Accepted Manuscript*, which has been through the Royal Society of Chemistry peer review process and has been accepted for publication.

Accepted Manuscripts are published online shortly after acceptance, before technical editing, formatting and proof reading. Using this free service, authors can make their results available to the community, in citable form, before we publish the edited article. We will replace this *Accepted Manuscript* with the edited and formatted *Advance Article* as soon as it is available.

You can find more information about *Accepted Manuscripts* in the Information for Authors.

Please note that technical editing may introduce minor changes to the text and/or graphics, which may alter content. The journal's standard Terms & Conditions and the Ethical guidelines still apply. In no event shall the Royal Society of Chemistry be held responsible for any errors or omissions in this *Accepted Manuscript* or any consequences arising from the use of any information it contains.

ROYAL SOCIETY OF CHEMISTRY

www.rsc.org/njc

New Journal of Chemistry

RSCPublishing

ARTICLE

Controllable synthesis of micro/nano-structured $MnCo_2O_4$ with multiporous core-shell architectures as high-performance anode materials for lithium-ion batteries

Xiaoyu Wu, Songmei Li*, Bo Wang, Jianhua Liu, Mei Yu

Cite this: DOI: 10.1039/x0xx00000x

Received 00th January 2012,
Accepted 00th January 2012

DOI: 10.1039/x0xx00000x

www.rsc.org/

Large-scale controllable synthesis of various micro/nano-structured $MnCo_2O_4$ is realized successfully via a facile hydrothermal method and the subsequent thermal annealing. Due to the effect of the triethanolamine (TEA) as surfactant, the obtained $MnCo_2O_4$ exhibit various micro/nano-structures (microellipses, microcubes, microspheres and twin microspheres), with unique core-shell architectures in which the microscale core is coated with multiporous shell composed of interconnected irregular nanoparticles. The formation mechanism of these unique structures is discussed in details. When evaluated as anode materials for lithium-ion batteries (LIBs), the as-prepared $MnCo_2O_4$ exhibit good electrochemical performance benefiting from the unique multiporous core-shell micro/nano-structures, which can effectively facilitate the charge transfer and Li^+ diffusion during the lithiation/delithiation process. Especially, the $MnCo_2O_4$ microspheres possess excellent lithium storage performance with high reversible capacity of 1033.3 mAh g^{-1} at a high current density of 400 mA g^{-1}, considerable capacity retention of 74.2% after 50 cycles, and remarkable rate capability, demonstrating the great potential as anode materials for high-performance LIBs.

Introduction

Nowadays, electrochemistry energy storage has become as one of the most essential topics for the whole world, thus it is urgent to develop some new types of efficient, clean and sustainable energy storage. Rechargeable lithium-ion batteries (LIBs) are considered as one of the most potential power sources for electric vehicles (EVs), hybrid electric vehicles (HEVs) and most of the portable electric devices. To meet the increasing requirements of practical applications, further improvements on LIBs in terms of cycling stability, energy density, rate capability, cost and safety are required. Therefore, extensive efforts have been focused on developing new advanced electrode materials, especially the anodes, for next-generation LIBs with high performance.[1-5]

Transition-metal oxides (TMOs), such as Co_3O_4, SnO_2, Fe_2O_3 and Mn_3O_4, have been widely investigated as candidates to replace conventional commercial graphite-based anode materials because of their high theoretical capacities and good chemical stabilities.[5-10] Recently, spinel binary transition-metal oxides, especially $MnCo_2O_4$, have attracted ever-increasing attention because of the better electronic conductivity than the single-metal oxides and the enhanced electrochemical performance by the complementarity and synergy of Co and Mn in the charge/discharge process.[11-16] To the best of our knowledge, researches on $MnCo_2O_4$ as anodes for LIBs are still in the infancy. Meanwhile, $MnCo_2O_4$ anodes still suffer severe capacity fading and poor rate capability, which is limited by the kinetics of ion diffusion and electronic conductivity, as well as the huge volume changes during the lithiation/delithiation process.[15] In order to further improve the lithium storage performance of $MnCo_2O_4$-based anode materials and facilitate their large-scale application, optimum structural design and the corresponding controllable synthesis could be the effective strategy and vital studying direction.

It is well-known that nanostructured electrode materials have attracted great interests because of their excellent lithium storage performance compared to the conventional bulk electrode materials, which is resulted from decreasing Li+ diffusion distances and increasing the contact area between the electro-active material and the electrolyte.[6,17-19] However, nanostructured electrode materials still suffer rapid capacity fading, which may be attributed to the severe self-aggregation caused by their high surface energy and the huge volume

*Key Laboratory of Aerospace Advanced Materials and Performance of Ministry of Education, School of Materials Science and Engineering, Beihang University, Beijing, 100191, China. E-mail: songmei_li@buaa.edu.cn; Fax: +86-10-82317103; Tel: +86-10-82317103

† Electronic supplementary information (ESI) available. See DOI:

changes of nanoparticles during Li^+ insertion and extraction process.[20-22] In this regard, micro/nano-structured materials with porous microstructures involving nanometer-sized subunits could be one of the optimal electrode materials for LIBs.[20-23] Especially, a stable microstructure with lower surface energy contributes to reducing the side reactions with the electrolyte, leading to improved cycling stability with few safety risks.[21] Typical multiporous structures are significant for relieving volume changes and improving the cycling stability. Meanwhile, the nanometer-sized subunits hold many advantages of nanostructured materials for high specific capacity and good rate performance. Therefore, in order to further improve the performances of LIBs, it is highly desirable to design multiporous micro/nano-structured electrode materials in the form of microscale particles assembled from nanoscale components as building blocks.[23,24]

Herein, we report a large-scale controllable synthesis of micro/nano-structured $MnCo_2O_4$ with multiporous core-shell architectures via a facile hydrothermal method and the subsequent thermal annealing. By adjusting the addition amount of the triethanolamine (TEA) as surfactant, various micro/nano-structured $MnCo_2O_4$ (microellipses, microcubes, microspheres and twin microspheres) are synthesized successfully. When tested as anode materials for LIBs, the micro/nano-structured $MnCo_2O_4$, especially the $MnCo_2O_4$ microspheres, exhibit high reversible capacity, excellent cycling stability and good rate capability, which could be attributed to the advantages of the unique multiporous core-shell micro/nano-structures.

Experimental

Chemicals

$Co(CH_3COO)_2 \cdot 4H_2O$, $Mn(CH_3COO)_2 \cdot 4H_2O$, $CO(NH_2)_2$ and $(HOCH_2CH_2)_3N$ (triethanolamine, abbreviated as TEA) are purchased from Beijing chemical Co., Ltd. (Beijing, China). All reagents used in the experiment were of analytical purity grade and used as received without further purification.

Controllable synthesis of micro/nano-structured $MnCo_2O_4$

In a typical process, $Co(CH_3COO)_2 \cdot 4H_2O$ (1.0 mmol), $Mn(CH_3COO)_2 \cdot 4H_2O$ (0. 5 mmol), $CO(NH_2)_2$ (4.0 g), and TEA (2 mL) were dissolved in 100 mL deionized water under constant magnetic stirring for 2 h. Then the solution was transferred into a Teflon-lined stainless steel autoclave (100 mL), and keeping sealed at 180 ℃ for 2.5 h. After hydrothermal reaction, the pink powders in the autoclave were collected and washed by deionized water and ethanol before being dried in a vacuum oven at 60 ℃ for 12 h. After that, a thermal annealing was performed in air at 600 ℃ for 8 h with a heating rate of 5 ℃ min^{-1}. Then, the black powders were obtained as final products for further characterization, which were denoted as MCO-2. By varying the addition amount of TEA to 4, 6, 8 mL, the other products were obtained and denoted as MCO-4, MCO-6 and MCO-8, respectively, directly corresponding to the amount of TEA used.

Materials Characterization

The crystallographic structures of the products were characterized by X-ray diffraction (XRD, Rigaku D/max-2200PC) equipped with Cu Kα radiation (λ=0.15418 nm), with the diffraction angle in the range of 10-80 °. The morphology and microstructure of the products were characterized by field-emission scanning electron microscope (FE-SEM, JEOL JSM-7500F) and transmission electron microscope (TEM, JEOL JEM-2100F). The elemental compositions of the products were analyzed by energy-dispersive X-ray spectroscope (EDS) equipped to FE-SEM and X-ray photoelectron spectroscopy (XPS, AXIS UTLTRADLD) equipped with a dual Mg Kα-Al Kα anode for photoexcitation. N_2 adsorption/desorption was measured using an ASAP-2010 surface area analyzer, and the pore size distribution was calculated from the adsorption branch of the isotherm.

Electrochemical measurements

Electrochemical measurements were performed at room temperature on 2025 coin-type cells assembled in an argon-filled glove box. The working electrodes were prepared by coating an N-methylpyrrolidinone (NMP) slurry composed of 70 wt. % active materials ($MnCo_2O_4$), 10 wt. % polyvinylidene fluoride (PVDF) and 20 wt. % acetylene black on copper foil current collectors followed by drying at 40 ℃ in vacuum oven for 12 h. The specific mass loading of the active materials for the working electrodes was about 1.2 mg cm^{-2}. Celgard 2400 was used as separator, and a solution of 1 M $LiPF_6$ dissolved in a 1:1 (v/v) mixture of ethylene carbonate (EC) and dimethyl carbonate (DMC) was used as electrolyte. The cyclic voltammetry (CV) and galvanostatic charge-discharge tests were conducted on LAND CT2001A battery-testing instrument and multichannel Arbin BT2000 system in the potential range of 0.005-3.0 V (vs. Li^+/Li) at room temperature. Electrochemical impedance spectroscopy (EIS) measurements were performed using an electrochemistry system (PARSTAT 2273, Princeton Applied Research, USA) by applying an AC voltage amplitude of 5 mV in the frequency range from 100 kHz to 50 mHz.

Results and discussion

The micro/nano-structured $MnCo_2O_4$ are synthesized by a facile hydrothermal method and the subsequent thermal annealing. The preparation process includes two steps. In the first step, the CoMn-precursor with well-defined microscale structure is formed under the effect of the TEA as surfactant during the hydrothermal reaction. Then the CoMn-precursor is converted to micro/nano-structured $MnCo_2O_4$ with multiporous core-shell architectures under the thermal annealing in air at 600 °C. With different addition amount of the TEA (2, 4, 6 and 8 mL), the formed $MnCo_2O_4$ shows various micro/nano-

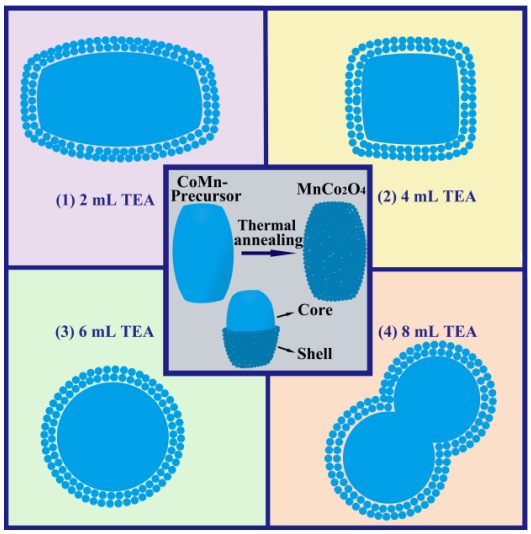

Fig. 1 Schematic illustration of the preparation process of various micro/nano-structured $MnCo_2O_4$.

structures (microellipse, microcube, microsphere and twin microspheres, respectively), as illustrated in Fig. 1.

Fig. 2 shows the X-ray diffraction (XRD) patterns of the CoMn-precursor and the final products. According to the XRD pattern in Fig. 2(a), the diffraction patterns of the CoMn-precursor are indexed as a mixture of hexagonal $CoCO_3$ (JCPDS no. 78-0209) and hexagonal $MnCO_3$ (JCPDS no. 85-1109), confirming the composition of the CoMn-precursor.[23] As shown in Fig. 2(b), it reveals that all the diffraction peaks of the products after thermal annealing could be easily indexed to the (111), (220), (311), (222), (400), (422), (511), (440), (620) and (533) crystal planes of the well-crystallized $MnCo_2O_4$ phase with cubic spinel structure, which is in agreement with the standard XRD pattern of cubic $MnCo_2O_4$ (JCPDS card no. 23-1237).[25-27] No peaks of impurities were detected, indicating the good crystallinity and purity of the as-prepared $MnCo_2O_4$. In addition, Fig. S1 (Supportiong Information) shows the similar XRD patterns of the four products, indicating the same composition of them.

The morphology and microstructure of the as-prepared $MnCo_2O_4$ with different addition amount of TEA were investigated by FE-SEM and TEM, as shown in Fig. 3. Obviously, the as-prepared $MnCo_2O_4$ show unique core-shell architectures, in which the microscale core is coated with multiporous shell composed of interconnected irregular nanoparticles. However, the MCO-2, 4, 6 and 8 products exhibit various micro/nano-structures of microellipses, microcubes, microspheres and twin microspheres, respectively. As shown in the SEM images in Fig. 3(a_1, a_2), $MnCo_2O_4$ microellipses of ~7μm in size with rough porous surface are obtained when the addition amount of TEA is 2 mL. However, when the addition amount of TEA is increased to 4 mL, multiporous microcubes are obtained as shown in Fig. 3(b_1, b_2), while the size of the microcubes is inhomogeneous with an average value of ~5μm. Moreover, the microspheres and twin microspheres with similar size of ~6μm are fabricated when the addition amount of TEA are increased to 6 mL and 8 mL, respectively, as shown in Fig. 3(c_1-c_2, d_1-d_2). The SEM images of the various micro/nano-stuctured $MnCo_2O_4$ with broken shells clearly show the core-shell architectures of the products (Fig. S2, Supporting Information). In order to further confirm the core-shell architectures of the various micro/nano-stuctured $MnCo_2O_4$ products, TEM images of the $MnCo_2O_4$ microellipses, microcubes, microspheres and twin microspheres are obtained and shown in Fig. 3(a_3-d_3), respectively. Obviously, all of the micro/nano-stuctured $MnCo_2O_4$ possess an obvious shell of 0.8-1.0 μm in thickness. In addition, the high-resolution transmission electron microscope (HRTEM) images of the $MnCo_2O_4$ twin microspheres are shown in Fig. S3 (Supporting Information). The lattice fringes with lattice spacings of 0.48 and 0.25 nm agree well with the (111) and (311) crystal planes of cubic phase $MnCo_2O_4$, corresponding with the XRD patterns shown in Fig. 2(b).

The composition of the products was confirmed by EDS analysis. According to the EDS spectrum in Fig. S4 (Supporting Information), the $MnCo_2O_4$ microspheres are mainly composed of Mn，Co and O elements, consisting with the XRD results. The EDS mapping images of the $MnCo_2O_4$ microspheres are shown in Fig. 4, roughly indicating the uniform distribution of Mn，Co and O elements in the $MnCo_2O_4$ products with core-shell micro/nano-structures. While the results of EDS line-scanning (Fig. S5, Supporting Information) indicate that the Mn concentration is obviously lower in the shell than in the core, which is resulted from the inherited concentration gradient controlled by the differential precipitation rates of $CoCO_3$ and $MnCO_3$ during the thermal annealing process.[23,28,29]

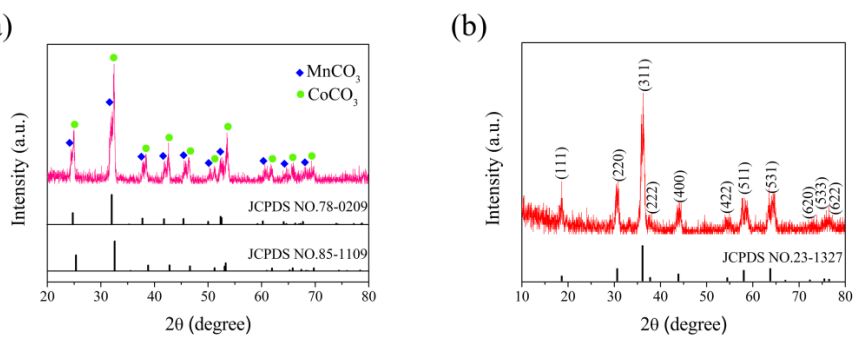

Fig. 2 XRD patterns of (a) the CoMn-precursor and (b) the MCO-6 products.

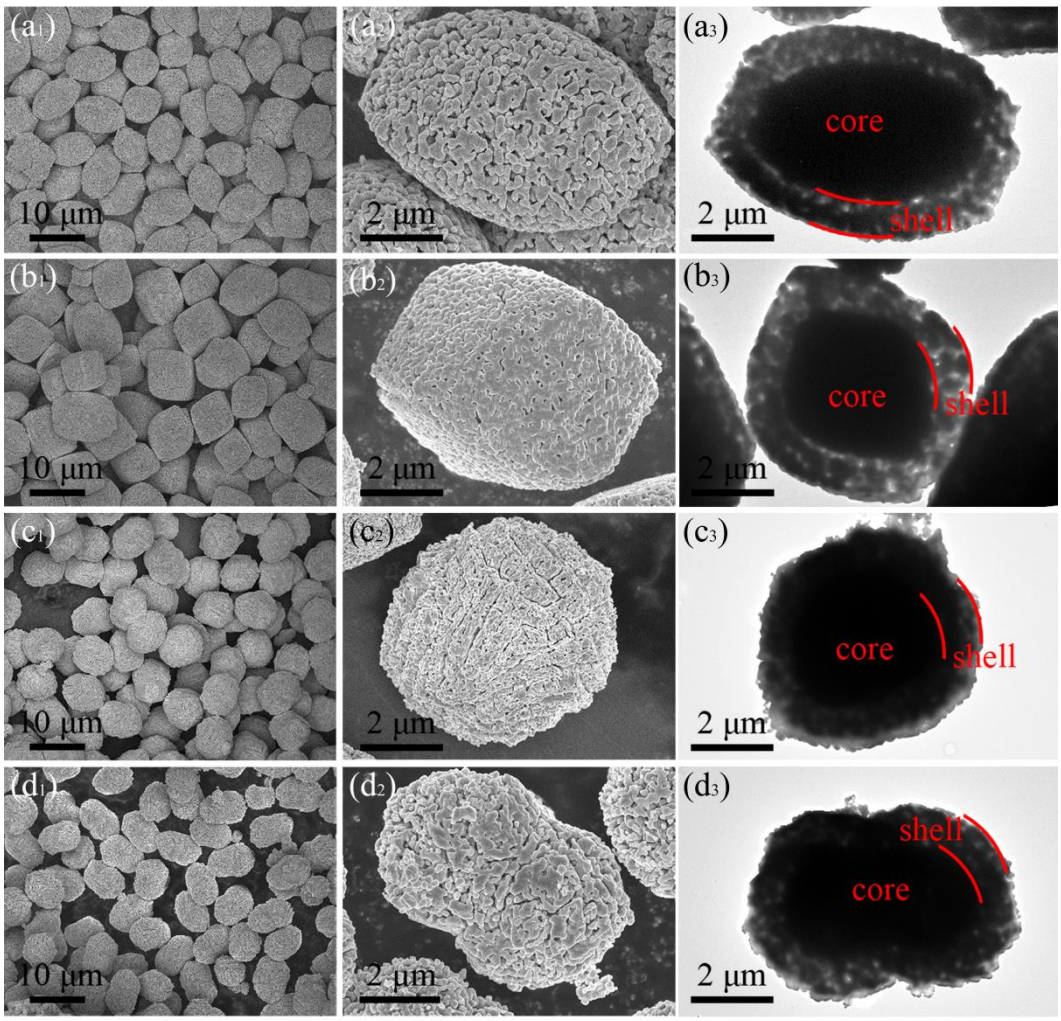

Fig. 3 (a_1-d_1, a_2-d_2) SEM and (a_3-d_3) TEM images of the various micro/nano-structured $MnCo_2O_4$. (a_1-a_3) MCO-2, (b_1-b_3) MCO-4, (c_1-c_3) MCO-6, and (d_1-d_3) MCO-8, respectively.

XPS analysis was carried out to demonstrate the detailed valence states of Mn and Co in the $MnCo_2O_4$ microspheres, in which C is used as a reference for normalization, and the results are shown in Fig. 5. All of the binding energies were corrected for specimen charging by normalizing them to the C 1s peak (set as 284.6 eV). The survey spectrum indicates the presence of O, Mn and Co, as well as C from the reference, and the absence of other impurities, as shown in Fig 5(a). According to the Gaussian fitting method, the Co 2p spectrum is best fitted considering two spin-orbit doublet characteristics of Co^{2+} and Co^{3+} and some shake-up satellites, while two main spin-orbit lines and little satellite could be observed in the Mn 2p spectrum.[16,30] After refined fitting, both of the spectra can be deconvoluted into four peaks as shown in Fig. 5(c, d), which exhibit the peak positions of the different valence states of Mn and Co clearly. Therefore, it is reasonable to conclude that Mn exists as Mn^{2+} and Mn^{3}+, meanwhile Co exists as Co^{2+} and Co^{3+} in the as-prepared $MnCo_2O_4$. In addition, the peaks at about 530.2 and 531.5 eV in the O 1s spectrum of Fig. 5(b) can be ascribed to the lattice oxygen in the $MnCo_2O_4$ phase and the oxygen of the hydroxide ions.[21]

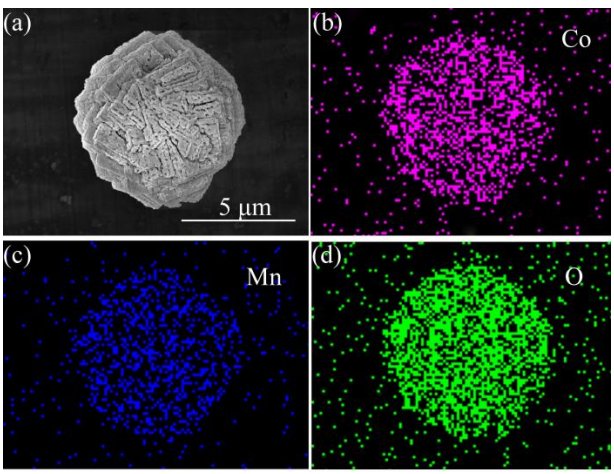

Fig. 4 EDS mapping images of the as-prepared $MnCo_2O_4$ microspheres.

Nitrogen absorption and desorption isotherms were collected to calculate the pore size distributions of the $MnCo_2O_4$ microspheres. According to the Barrett-Joyner-

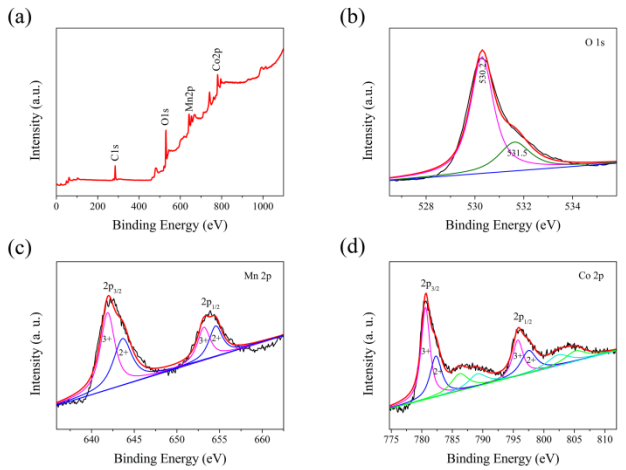

Fig. 5 XPS spectra of (a) survey spectrum, (b) O 1s, (c) Mn 2p, and (d) Co 2p for the $MnCo_2O_4$ microspheres.

Halenda (BJH) pore size distribution shown in Fig. S6 (Supporting Information), a sharp peak at the pore size range of 2-5 nm can be seen clearly, which is attributed to the mesoporous channels in $MnCo_2O_4$ microspheres, thus confirming the multiporous structure of the products.[23,25,31] Generally speaking, multiporous structure is optimal for lithium storage behavior, which is beneficial to the transport and diffusion of ions since the nanoscale pores can facilitate penetration of the electrolyte and ions through bulky electrodes.[32]

Based on the above results, the possible formation mechanism of the various micro/nano-structured $MnCo_2O_4$ is concluded and illustrated in Fig. 6. During the hydrothermal reaction, the $CoCO_3$ and $MnCO_3$ composites with well-defined microscale structures as precursors are formed under the appropriate hydrothermal condition and the influence of the special weak alkaline surfactant.[23] In detail, at the primary stage of hydrothermal reaction, irregular $CoCO_3$ and $MnCO_3$ particles

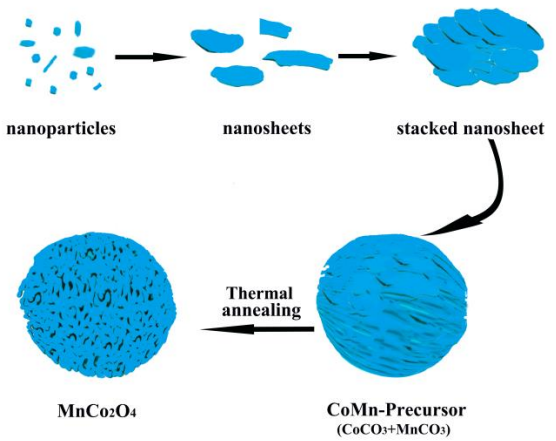

Fig. 6 Schematic illustration of the formation mechanism of the micro/nano-structured $MnCo_2O_4$.

as crystal nuclei are formed when the pH of the reaction system is increased by the slow hydrolysis of $CO(NH_2)_2$ and CO_3^{2-} anions are released gradually. And the particles are induced to grow to sheets on account of the preferred orientation growth of hexagonal $CoCO_3$ and $MnCO_3$.[24,33] As the reaction progressed, the primary structures are formed through the self-assembly of sheets to reduce the interfacial energy. In the latter stage of the hydrothermal reaction, due to the impact of the surfactant (TEA) which has a favorable interaction with the Co^{2+}, Mn^{2+} and the precipitated particles, the stacked sheets continue to grow up to the precursors with well-defined microscale structures. Remarkably, the addition amount of the TEA plays a key role in controlling the shapes of the products. After hydrothermal reaction, the decomposition reaction and release of CO_2 lead to the formation of multiporous shell when the CoMn-precursors are under thermal annealing in air at 600 °C, thus converting the CoMn-precursors to micro/nano-structured $MnCo_2O_4$ with multiporous core-shell architectures.[24,34,35] The formation mechanism can be expressed as the following reactions:[23]

$$CO(NH_2)_2 + 2H_2O \rightarrow 2NH_4^+ + CO_3^{2-} \quad (1)$$

$$Mn^{2+} + CO_3^{2-} \rightarrow MnCO_3\downarrow \quad (2)$$

$$Co^{2+} + CO_3^{2-} \rightarrow CoCO_3\downarrow \quad (3)$$

$$2MnCO_3 + 4CoCO_3 + O_2 \rightarrow 2MnCo_2O_4 + 6CO_2 \quad (4)$$

The micro/nano-structured $MnCo_2O_4$ exhibits remarkable electrochemical performances as anode materials for LIBs, as shown in Fig. 7. Cyclic voltammetry (CV) measurements were conducted to identify the electrochemical reactions occurred during the lithiation/delithiation process of the $MnCo_2O_4$ electrode. Fig. 7(a) shows the initial four cyclic voltammetry (CV) curves of the $MnCo_2O_4$ microspheres electrode at a scan rate of 0.1 mV s^{-1} between 0.005 and 3.0 V (vs. Li^+/Li). In the first cathodic scan, an intense peak is observed at ~0.53 V, which can be assigned to the reduction of $MnCo_2O_4$ to Mn and Co, as well as the decomposition of organic electrolyte to form a solid electrolyte interphase (SEI) layer at the electrode-electrolyte interface.[31,36] In the first anodic scan, a broad peak in the range of 1.7-2.3 V can be observed, which is usually ascribed to the oxidation of Mn and Co. In the second and following cycles, the main cathodic peak is moved to ~1.02 V, corresponding to the reduction of Mn^{2+} and Co^{2+}. Obviously, the CV curves of the second and following cycles are different from that of the first cycle, while the second and following CV curves are almost overlapped, presenting excellent reversible performances except for the irreversible reactivity in the first cycle.[21,31] Therefore, on the basis of above analysis, the electrochemical reactions of the $MnCo_2O_4$ electrodes can be described as follows:[23,31,37]

$$MnCo_2O_4 + 8Li^+ + 8e^- \rightarrow Mn + 2Co + 4Li_2O \quad (5)$$

$$Mn + 2Co + 3Li_2O \leftrightarrow 2CoO + MnO + 6Li^+ + 6e^- \quad (6)$$

The electrochemical performance of the various micro/nano-structured $MnCo_2O_4$ have been further examined by galvanostatic charge-discharge tests at a current density of 400 mA g^{-1} in the potential range of 0.005-3.0 V (vs. Li^+/Li). The charge-discharge profiles of the $MnCo_2O_4$ microspheres electrode in the 1st, 2nd, 3rd, 4th and 50th cycles are shown in Fig. 7(b). The initial charge and discharge capacities of the electrode are 1075.0 and 1425.8 mAh g^{-1}, respectively, corresponding to an initial Coulombic efficiency of 75.4%. The initial capacity loss of the electrode can be mainly ascribed to the difficult dissolution of the SEI layers and the incomplete decomposition of Li_2O, as well as the irreversible lithium loss.[37,38] Meanwhile, compared to the theoretical capacity (906 mAh g^{-1}) of $MnCo_2O_4$ calculated on the basis of equation (5), the extra capacity at the first discharge may resulted from the formation of SEI layers on the electrode-electrolyte interface.[21,37,39] In the second cycle, the discharge and charge capacities of the $MnCo_2O_4$ microspheres electrodes are 1033.3 and 1008.3 mAh g^{-1} respectively. And the Coulombic efficiency rapidly rises to 97.5% and then increase gradually to about 99% in the subsequent cycles. Compared to the $MnCo_2O_4$ microellipses, microcubes and twin microspheres electrodes, whose charge-discharge profiles are shown in Fig. S7 (Supporting Information), the $MnCo_2O_4$ microspheres electrode exhibits higher reversible capacity, indicating its superior electrochemical performance among them.

Moreover, the various micro/nano-structured $MnCo_2O_4$, especially the $MnCo_2O_4$ microspheres, exhibit excellent cycling performance as shown in Fig. 7(c), which were tested at a current of 400 mA g^{-1} for 50 cycles in the voltage range of 0.005-3.0 V (vs. Li^+/Li). As shown in Fig. 7(c), after 50 cycles, the $MnCo_2O_4$ microellipses, microcubes and twin microspheres maintain high capacities of 616.7, 658.3 and 700.0 mAh g^{-1} respectively. For $MnCo_2O_4$ microspheres, the reversible capacities from the 2nd cycle to the 30th cycle decrease slowly and gradually reach a stable value of ~835 mAh g^{-1}. After 50 cycles, the reversible capacity of $MnCo_2O_4$ microspheres maintains as high as 766.7 mAh g^{-1}, which is higher than these of $MnCo_2O_4$ microellipses, microcubes and twin microspheres, with the capacity retention ratio of 74.2%. The superior cycling performance of the microspheres compared to that of other structures may be ascribed to their unique surface morphology with obvious ordered ditches (Fig. S8, Supporting Information), and the excellent structural stability resulted from the regular spherical shape. In addition, the reversible capacity and cycling stability of the various micro/nano-structured $MnCo_2O_4$, especially $MnCo_2O_4$ microspheres, are outstanding compared to that of $MnCo_2O_4$-based anode materials reported in the previous literatures, such as the multiporous $MnCo_2O_4$ spinel quasi-hollow spheres (the capacity is maintained at 755 mAh g^{-1} after 25 cycles at the current density of 200 mA g^{-1}),[15] the core-shell ellipsoidal $MnCo_2O_4$ (the reversible capacity goes down to ~620.0 $mAhg^{-1}$ at the 50th cycle when the current density is 400 mA g^{-1}),[23] and the $MnCo_2O_4$ octahedral structure (the reversible capacity maintains 618 mA hg^{-1} after 50 cycles at 0.1 C).[40]

Furthermore, the rate capability of the $MnCo_2O_4$ microspheres electrode is shown in Fig. 7(d). To perform the rate capability measurements, the electrode was charged and discharged for 10 cycles at different current densities from 100

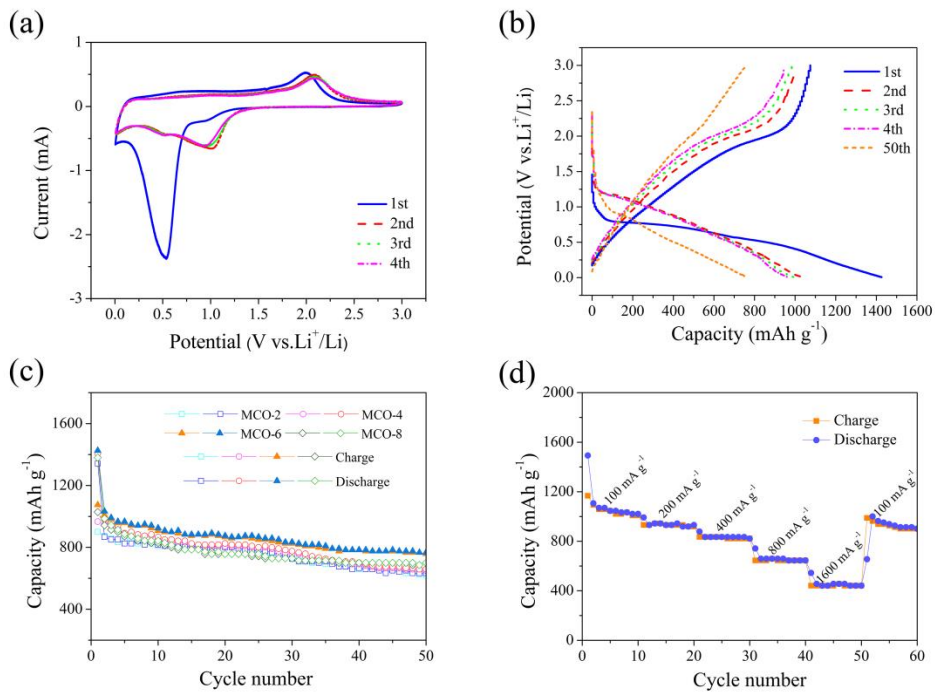

Fig. 7 (a) Cyclic voltammograms of the $MnCo_2O_4$ microspheres electrode for the initial four cycles at a scan rate of 0.1 mV s^{-1} in the voltage range of 0.005-3.0 V; (b) Charge-discharge voltage profiles of the $MnCo_2O_4$ microspheres electrode at a current density of 400 mA g^{-1}; (c) Comparison of cycling performance of the various micro/nano-structured $MnCo_2O_4$ electrodes at a current density of 400 mA g^{-1}; (d) Rate capability of the $MnCo_2O_4$ microspheres electrode.

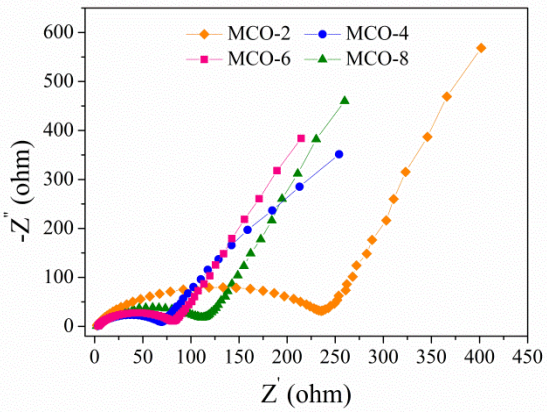

Fig. 8 Nyquist plots of the various micro/nano-structured $MnCo_2O_4$ electrodes in the frequency range from 100 kHz to 50 mHz.

to 1600 mA g^{-1}, and finally returned to 100 mA g-^{1}. From Fig. 7(d), it can be seen that the average discharge capacities of the microspheres electrode at different current densitiies of 100, 200, 400 and 800 mA g-1 are 1093.9, 938.7, 837.6 and 661.6 mAh g^{-1}, respectively. Even at a high current density of 1600 mA g^{-1}, the capacity retains at 457.4 mAh g^{-1}. More importantly, when the current density returns back to the initial 100 mA g^{-1} after 50 cycles, the capacity of the $MnCo_2O_4$ microspheres electrode could be recovered close to its initial value, indicating the good reversibility and rate performance of the electrode.

To further clarify the superior electrochemical performance of the $MnCo_2O_4$ miscrospheres, EIS measurements were performed on the various micro/nano-structured $MnCo_2O_4$ electrodes. Fig. 8 shows the Nyquist plots of the various micro/nano-structured $MnCo_2O_4$ electrodes in the frequency range from 100 kHz to 50 mHz. It can be seen that the Nyquist plots are all composed of semicircles in middle and high frequencies, which are often considered to be the superposition of two individual semicircles, and slope lines in low frequencies. The semicircle at high-frequency region is attributed to the formation of the SEI layer and contacting impedance between active materials and electrolyte.[24,41] The semicircle in the middle frequency range can be assigned to the charge-transfer resistance (R_{ct}), relating to charge transfer through the electrode–electrolyte interface.[41,42] And the slope line in low-frequency region represented the Warburg impedance (Z_w), which is related to the diffusion-controlled process in the solid state electrodes.[24,41-43] Obviously, the diameters of the semicircles for the MCO-4 and MCO-6, corresponding to the as-prepared $MnCo_2O_4$ microcubes and microspheres respectively, are smaller than that of the $MnCo_2O_4$ microellipses and twin microspheres (MCO-2 and MCO-8, respectively), suggesting that the $MnCo_2O_4$ microcubes and microspheres have lower contact and charge-transfer impedances. Meanwhile, more vertical line in low-frequency region of the $MnCo_2O_4$ microspheres compared to the microcubes indicates the faster Li^+ diffusion behavior of the $MnCo_2O_4$ microspheres, thereby resulting in the better electrode reaction kinetics during the charge/discharge process and superior cycling performance of the $MnCo_2O_4$ microspheres electrodes as mentioned above.

The enhanced electrochemical performance for these $MnCo_2O_4$ samples, especially $MnCo_2O_4$ microspheres, could be attributed to their unique multiporous core-shell micro/nano-structures. Firstly, the multiporous structure composed of nanoparticles effectively shortens the pathway for Li^+ diffusion and offers a large-area contact for material and electrolyte, which may accelerate the charge transfer and thus contribute to the better rate capability. Meanwhile, the nanoscale interspaces between nanoparticles provide abundant spaces to accommodate the volume changes during the charge/discharge process, devoting to enhanced cycling performance. Furthermore, the unique core-shell structure with regular core coated by multiporous shell could significantly enhance the structural integrity by partially mitigating the mechanical strain associated with the repeated Li^+ insertion/extraction processes during cycling, thus improving the cycling stability.[15,21] It is noteworthy that the $MnCo_2O_4$ microspheres exhibit the best structural superiority with the best electrode reaction kinetics, thereby possessing the best lithium storage performance among the various micro/nano-structured $MnCo_2O_4$.

Conclusions

In summary, various micro/nano-structured $MnCo_2O_4$ (microellipses, microcubes, microspheres and twin microspheres) have been synthesized controllably through a facile hydrothermal method and the subsequent thermal annealing. All of the obtained $MnCo_2O_4$ show unique multiporous core-shell micro/nano-structure, in which the microscale core is coated with mesoporous shell composed of interconnected irregular nanoparticles. Remarkably, the triethanolamine used as surfactant plays a key role in shape-controlling of the products during the hydrothermal process. Benefiting from the unique multiporous core-shell micro/nano-structure, which effectively facilitate the charge transfer and Li^+ diffusion during the lithiation/delithiation process, the micro/nano-structured $MnCo_2O_4$ electrodes exhibit enhanced lithium storage performance. Especially, the $MnCo_2O_4$ microsphere electrodes possess high reversible capacity of 1033.3 mAh g^{-1} at the current density of 400 mA g^{-1}, enhanced cycling performance with the capacity maintaining as 766.7 mAh g^{-1} after 50 cycles and good rate capability.

Acknowledgements

This work was supported by the National Natural Science Foundation of China (Grant No. 51271012).

References

1 M. Armand, and J. M. Tarascon, *Nature*, 2008, **451**, 652.
2 J. Cabana, L. Monconduit, D. Larcher, and M. R. Palac ń, *Adv. Mater.*, 2010, **22**, E170.
3 L. W. Ji, Z. Lin, M. Alcoutlabi, and X. W. Zhang, *Energy Environ. Sci*,

2011, **4**, 2682.
4 R. Marom, S. F. Amalraj, N. Leifer, D. Jacob, and D. Aurbach, *J. Mater. Chem.*, 2011, **21**, 9938.
5 H. B. Wu, J. S. Chen, H. H. Hng, X. W. D. Lou, *Nanoscale*, 2012, **4**, 2526.
6 P. Poizot, S.Laruelle, S. Grugeon, L. Dupont, and J. M. Tarascon, *Nature*, 2000, **407**, 496.
7 C. Cheng, G. Zhou, J. Du, H. M. Zhang, D. Guo, Q. H. Li, W. F. Wei, and L. B. Chen, *New J. Chem.*, 2014, **38**, 2250.
8 X. M. Ye, W. J. Zhang, Q. J. Liu, S. P. Wang, Y. Z. Yang, and H. Y. Wei, *New J. Chem.*, 2015, **39**, 130.
9 H. Liu, G. Wang, J. Park, J.cZ. Wang, H. K. Liu, and C. Zhang, *Electrochim. Acta*, 2009, **54**, 1733.
10 Q. M. Pan, and J. Liu, *J. Solid State Electrochem.*, 2009, **13**, 1591.
11 J. F. Li, J. Z. Wang, D. Wexler, D. Q. Shi, J. W. Liang, H. K. Liu, S. L. Xiong, and Y. T. Qian, *J. Mater. Chem. A*, 2013, **1**, 15292.
12 B. Cui, H. Lin, J. B. Li, X. Li, J. Yang, and J. Tao, *Adv. Funct. Mater.*, 2008, **18**, 1440.
13 Z. H. Li, T. P. Zhao, X. Y. Zhan, D. S. Gao, Q. Z. Xiao, and G. T. Lei, *Electrochim. Acta*, 2010, **55**, 4594.
14 H. X. Zhao, Z. Zheng, K. W. Wong, S. M. Wang, B. J. Huang, and D. P. Li, *Electrochem. Commun.*, 2007, **9**, 2606.
15 J. F. Li, S. L. Xiong, X. W. Lia, Y. T. Qian, *Nanoscale*, 2013, **5**, 2045.
16 X. J. Hou, X. F. Wang, B. Liu, Q. F. Wang, T. Luo, D. Chen, and G. Z. Shen, *Nanoscale*, 2014, **6**, 8858.
17 K. X. Wang, X. H. Li, and J. S. Chen, *Adv. Mater.*, 2015, **27**, 527.
18 G. Centi, and S. Perathoner, *Eur. J. Inorg. Chem.*, 2009, **26**, 3851.
19 Y. G. Wang, H. Q. Li, P. He, E. J. Hosono, and H. S. Zhou, *Nanoscale*, 2010, **2**, 1294.
20 L. Hu, H. Zhong, X. R. Zheng, Y. M. Huang, P. Zhang, and Q. W. Chen, *Scientific reports*, 2012, **2**, 986.
21 J. Bai, X. G. Li, G. Z. Liu, Y. T. Qian, and S. L. Xiong, *Adv. Funct. Mater.*, 2014, **24**, 3012.
22 A. S. Arico`, P. Bruce, B. Scrosati, J. M. Tarascon, and W. V. Schalkwijk, *Nat. Mater.*, 2005, **4**, 366.
23 G. Y. Huang, S. M. Xu, Z. H. Xu, H. Y. Sun, and L. Y. Li, *Appl. Mater. Interfaces*, 2014, **6**, 21325.
24 G. Y. Huang, S. M. Xu, S. S. Lu, L. Y. Li, and H. Y. Sun, *Electrochim. Acta*, 2014, **135**, 420.
25 A. K. Mondal, D. W. Su, S. Q. Chen, A. Ung, H. S. Kim, and G. X. Wang, *Chem. Eur. J.*, 2015, **21**, 1526.
26 S. C. Ma, L. Q. Sun, L. N. Cong, X. G. Gao, C. Yao, X. Guo, L. H. Tai, P. Mei, Y. P. Zeng, H. M. Xie, and R. S. Wang, *J. Phys. Chem. C*, 2013, **117**, 25890.
27 M. Y. Qiu, S. H. Zhan, H. B. Yu, D. D. Zhu, and S. Q. Wang, *Nanoscale*, 2015, **7**, 2568.
28 Y. K. Sun, B. R. Lee, H. J. Noh, H. M. Wu, S. T. Myung and K. Amine, *J. Mater. Chem.*, 2011, **21**, 10108.
29 Y. K. Sun, D. H. Kim, C. S. Yoon, S. T. Myung, J. Prakash and K. Amine, *Adv. Funct. Mater.*, 2010, **20**, 485.
30 T. Y. Ma, Y. Zheng, S. Dai, M. Jaroniec, and S. Z. Qiao, *J. Mater. Chem. A*, 2014, **2**, 8676.
31 J. F. Li, J. Z. Wang, X. Liang, Z. J. Zhang, H. K. Liu, Y. T. Qian, and S. L. Xiong, *ACS Appl. Mater. Interfaces*, 2014, **6**, 24.
32 L. Li, F. He, S. L. Gai, S. H. Zhang, P. Gao, M. L. Zhang, Y. J. Chen, and P. P. Yang, *CrystEngComm.*, 2014, **16**, 9873.
33 F. Cao, D. Q. Wang, R. P. Deng, J. K. Tang, S. Y. Song, Y. Q. Lei, S. Wang, S. Q. Su, X. G. Yang, and H. J. Zhang, *CrystEng Comm.*, 2011, **13**, 2123.
34 G. Y. Huang, S. M. Xu, S. S. Lu, L. Y. Li, and H. Y. Sun, *ACS Appl. Mater. Interfaces*, 2014, **6**, 7236.
35 W. W. Yuan, D. Xie, Z. M. Dong, Q. M. Su, J. Zhang, G. H. Du, and B. S. Xu, *Mater. Lett.*, 2013, **97**, 129.
36 Y. Sharma, N. Sharma, G. V. Subba Rao, and B. V. R. Chowdari, *Adv. Funct. Mater.*, 2007, **17**, 2855.
37 J. F. Li, S. L. Xiong, X. W. Li, and Y. T. Qian, *Nanoscale*, 2013, **5**, 2045.
38 D. Zhao, Y. Xiao, X. Wang, Q. Gao, and M. H. Cao, *Nano Energy*, 2014, **7**, 124.
39 L. Yu, L. Zhang, H. B. Wu, G. Q. Zhang, and X. W. D. Lou, *Energy Environ. Sci.*, 2013, **6**, 2664.
40 L. F. Duan, F. H. Gao, L. M. Wang, S. Z. Jin, and H. Wu, *J. Adv. Ceramics*, 2013, **2**, 266.
41 D. Aurbach, *J. Power Sources*, 2000, **89**, 206.
42 B. Wang, S. M. Li, J. H. Liu, M. Yu, B. Li, and X.Y. Wu, *Electrochim. Acta*, 2014, **146**, 679.
43 K. M. Shaju, F. Jiao, A. Débart, and P. G. Bruce, *Phys. Chem. Chem. Phys.*, 2007, **9**, 1837.

Graphical Abstract

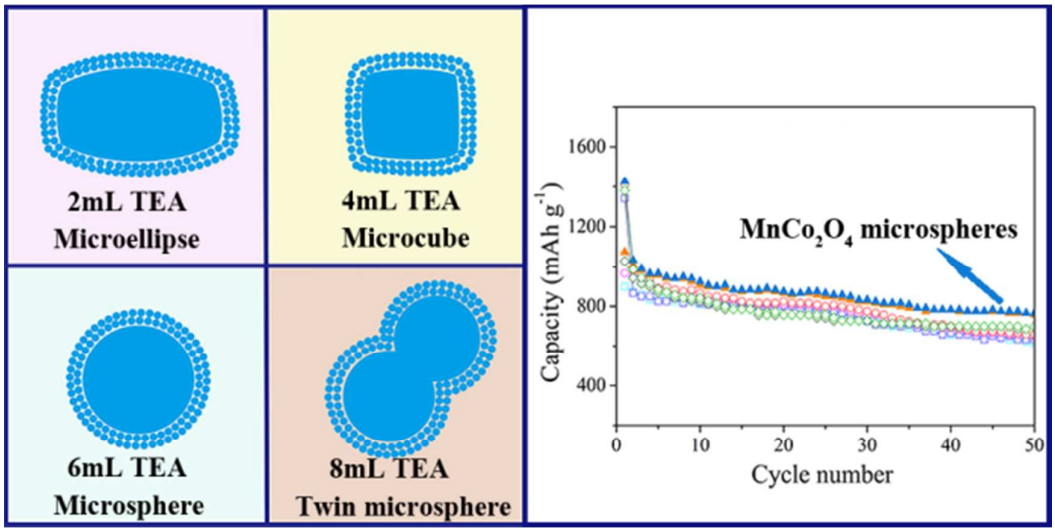

Various micro/nano-structured $MnCo_2O_4$ with excellent lithium storage performance were synthesized controllably.